Sensors & Actuators: B. Chemical 357 (2022) 131458

Contents lists available at ScienceDirect

Sensors and Actuators: B. Chemical

journal homepage: www.elsevier.com/locate/snb

All-electrical antibiotic susceptibility testing within 30 min using silicon nano transistors

Xingxing Xu [a], Si Chen [a], Yingtao Yu [a], Petra Virtanen [b], Jiyue Wu [a], Qitao Hu [a], Sanna Koskiniemi [b,*], Zhen Zhang [a,*]

[a] Division of Solid-State Electronics, Department of Electrical Engineering, Ångström Laboratory, Uppsala University, SE-75103 Uppsala, Sweden
[b] Department of Cellular and Molecular Biology, Uppsala University, SE-75124 Uppsala, Sweden

ARTICLE INFO

Keywords:
Antibiotic susceptibility testing
Point of care
Minimal inhibitory concentration
Ion-selective field-effect transistor
Cell metabolism

ABSTRACT

Rapid and reliable antibiotic susceptibility testing (AST) platform is highly desired to select the right antibiotics to treat infectious disease at early stage. Here, we demonstrate rapid ASTs using nanoscale silicon ion-selective field-effect transistor sensors. Our sensors profile bacterial metabolic kinetics by monitoring the metabolism induced acidification in the growth media with the absence and the presence of different antibiotics. Rapid AST results could be determined from the metabolic profiles with a total assay time less than 30 min for different bacterial strains. In addition, the sensors could also distinguish the bactericidal mechanisms for antibiotics with different modes of actions. Furthermore, the initial bacterial concentration in an unknown sample, a key parameter to determine its clinic relevance, could be estimated based on the metabolic profiles. Our demonstrated AST method is all-electrical, label-free and silicon technology compatible, and holds great promise for the development of a high-throughput and low-cost point-of-care device.

1. Introduction

For most infectious diseases, early and effective treatment is crucial to avoid costly and perhaps even lethal complications. However, the emergence of antimicrobial resistance (AMR) has made effective treatment of bacterial infections difficult and become one of the biggest threats to global health [1–4]. It is estimated that deaths from drug-resistant infections will increase from currently 700,000–10 million worldwide each year by 2050, unless a global response is mounted [5]. The increasing prevalence of drug-resistant bacteria in the community forces physicians to either risk treatment failure with older antibiotics or use effective last-resort antibiotics. A more preventive approach is to perform antibiotic susceptibility testing (AST) prior to drug administration, which will allow physicians to select the most effective drugs. AST not only reduces the risk of severe infection for patients, but also prevents the increased usage of last-resort antibiotics which will rapidly drive resistance also to these drugs [6–8].

The most widely used reliable tests in clinical practice are phenotypic ASTs, which typically monitor the proliferation of bacteria in presence of antibiotics [8–10]. However, the currently employed phenotypic ASTs in clinics normally need tens of generations of growth and usually take more than two days [8], [11]. Even with the most recent rapid AST protocol [11], for many infections, the traditional test still takes too long for patients to wait for therapy. In contrast to phenotypic ASTs, genotypic ASTs are based on the direct detection of specific genetic markers associated with resistance (resistance genes, mutations) using standard molecular biology tools such as polymerase chain reaction (PCR). Although genotypic ASTs can perform rapid detection within a few hours [12], [13], the presence of a resistance gene is however not always associated with the actual resistance, which will lead to false positives. In addition, genotypic ASTs are not able to detect new and previously unidentified resistance mechanisms. Therefore, achieving rapid and reliable AST on a phenotypic platform is of great importance for infection treatments.

During the past decade, there has been significant advancements in the development of rapid AST approaches, in an effort to curtain the widespread of antibiotic-resistant infections. These approaches involved a variety of mechanisms to detect bacteria response to antibiotics, including mechanical vibrations [14], impedance [15], metabolic byproducts [16], high-resolution imaging [17], [18], etc. However, despite the immense scientific potential, each of these emerging technologies comes with some drawbacks, and their adaptability into the

* Corresponding authors.
E-mail addresses: sanna.koskiniemi@icm.uu.se (S. Koskiniemi), zhen.zhang@angstrom.uu.se (Z. Zhang).

https://doi.org/10.1016/j.snb.2022.131458
Received 25 October 2021; Received in revised form 18 January 2022; Accepted 19 January 2022
Available online 21 January 2022

real clinical workflow remains to be seen. Among different detection methods, electrical sensing is very attractive for their potential advantages such as small-size and weight, high reliability, and possibility of high density on-chip integration of sensors and signal processing electronics [19–21]. Their compatibility with the standard silicon complementary metal-oxide-semiconductor (CMOS) technology also holds great promise for developing a point-of-care (POC) device which can be produced with low-cost. Such feature is essential for AST in remote or less developed regions where laboratory resources are limited.

Previous work on electrical ASTs commonly used, for example, impedance changes as a measure of bacterial cell response to antibiotics and to determine the susceptibility [15], [21]. When combined with microfluidics, impedance-based AST system can analyze bacterial cells with high throughput and deliver AST results within an hour [15]. However, impedance measurement is prone to coupling of parasitic elements in the circuit between the lead contacts and the culture liquid or the bacterial cytoplasmic matrix. For example, the impedance contributed by the solid-liquid interface, is very sensitive to the electrode surface conditions and may dominate the total measured impedance [22]. Therefore, impedance data interpretation normally requires complex circuit modeling taking into considerations geometric and electrical parameters of bacterial cells, electrode surface conditions, and their surrounding microfluidic channel.

Live bacterial cells require energy to maintain transmembrane ionic gradients and to sustain cell growth [23]. In the presence of glucose, the metabolic products of *Escherichia coli* (*E. coli*) and many other bacterial strains change the *p*H of the surrounding growth media [16]. In this work, we present a fully electrical AST approach based on ion-selective silicon nanowire field-effective transistor (SiNWFET) sensors. The sensors monitor cell metabolic activity by specifically measuring the H^+ ions generated by bacterial metabolism. Adsorption and desorption of H^+ ions on the SiNWFET sensor surface can lead to a change in surface potential and hence a change in its threshold voltage (V_T) [20]. A highly H^+-selective sensing oxide layer wrapping the SiNWFET channel ensures reliable detection of tiny H^+ concentration changes even with a high background ionic concentration. By employing standard silicon process technology, performance variations among different SiNWFET sensors are minimized, which is critical for parallelization of multiple ASTs on a single chip. In addition, the data interpretation is straight forward as the readout signal, i.e., V_T shift (ΔV_T), of the SiNWFET sensor correlates linearly with the *p*H of the culture medium.

In following sections, we demonstrate that SiNWFET sensors can deliver AST results for *E. coli* with a total assay time of less than 30 min. Rapid AST for *E. coli* has important clinical impact because *E. coli* is responsible for 85% of the urinary tract infection (UTI) cases diagnosed in primary care. In addition, rapid ASTs are also achieved for other pathogen species such as Gram-positive *Staphylococcus aureus* (*S. aureus*) and *Staphylococcus saprophyticus* (*S. saprophyticus*). Apart from the fast readout, the sensors could also differentiate the bactericidal mechanisms of the antibiotics as well as the metabolic patterns of different bacteria species. Our sensors could also quantify the cell density in an unknown bacterial sample based on the measured metabolic profile since the acidification rate of culturing solution and bacterial density are strongly correlated [24]. Finally, we develop an analytical model for quantitative extraction of metabolic kinetic parameters during bacteria growth.

2. Materials and methods

2.1. Fabrication of SiNWFET sensors

The SiNWFETs were fabricated on a silicon-on-insulator (SOI) wafers using standard silicon process technology. Fig. 1a shows a photo image of an AST chip with 24 SiNWFET sensors. Scanning electron microscopy (SEM) images of a SiNWFET sensor along with a zoomed-in view of the SiNW channel region are shown in Fig. 1b. The SOI wafers comprised a 200-nm-thick lightly p-type doped silicon layer on top of a 375-nm-thick buried oxide (BOX). The top silicon layer was firstly thinned down to 120 nm via thermal oxidation. Source/drain (S/D) regions of the SiNWFETs were heavily n-doped by arsenic (As) implantation (energy =

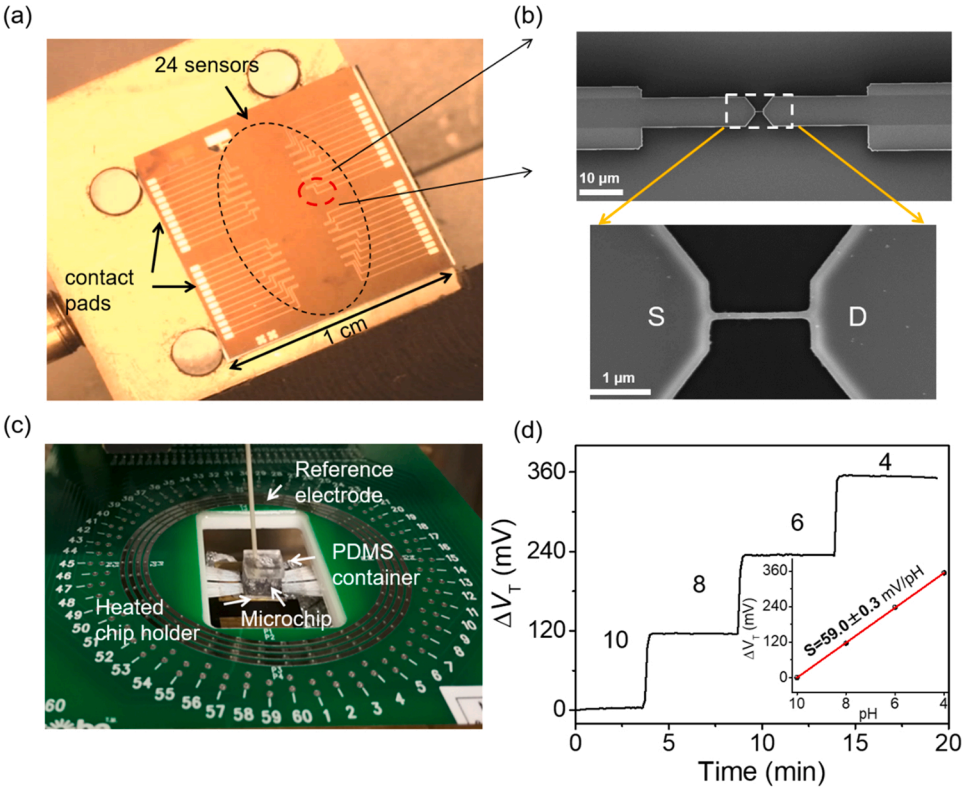

Fig. 1. (a) photo image of a chip containing 24 SiNWFET sensors, placed on a temperature-controlled chip holder, (b) SEM images of a SiNWFET (upper) and its zoomed-in channel region (lower), (c) experimental arrangement for real-time monitoring of culture medium acidification induced by bacterial metabolism, and (d) ΔV_T vs. t curve for a SiNWFET measured in buffer solutions with *p*H changing from 10 to 4. The *p*H values were annotated on the curve. Inset: SiNWFET sensitivity calibration curve, i.e., ΔV_T vs. *p*H. Note that each data point is averaged from three independent measurements and error bars representing standard deviations are also included in the inset.

30 keV, dose = 5 $\times 10^{15}$ cm^{-2}) while the channel region was protected by photoresist during the implantation. The device structure including S/D pads and SiNW channel was defined by electron beam lithography (EBL) and subsequent reactive ion etching (RIE). To further reduce the contact resistance to S/D, a 5-nm-thick Ni layer was deposited on the S/D via lift-off and subsequently annealed at 400 °C in N_2 for 30 s using rapid thermal process (RTP) to form NiSi. Afterward, a 5-nm-thick HfO_2 was grown by atomic layer deposition (ALD, R200 unit, Picosun) at 170 °C to serve as the gate dielectric as well as the passivation layer for liquid operation. The S/D contact pads along the chip edges were metallized with bilayer of 10 nm Ti and 100 nm Al. Finally, forming gas annealing (FGA) was performed in diluted H_2 (5% H_2 in N_2, 400 °C, 30 min) to neutralize the SiNW channel/gate oxide interface traps.

2.2. Electrical measurement

The electrical measurements were performed using HP4155A semiconductor parameter analyzer. 4 SiNWFETs were measured simultaneously using a switch unit (Keithley 34970 A). A schematic view of the measurement setup is shown in Fig. 1c. The chip holder is connected with a thermocouple in order to maintain the measurement solution at 37 ℃. A drop of mine oil was covered on the measurement solution to reduce the evaporation during measurement. The transfer curve was first measured. The I_{DS} was then monitored in real-time with a constant source-drain voltage (V_{DS}) at 1 V and a constant gate voltage (V_G) applied with respect to an Ag/AgCl/KCl reference electrode (Warner Instruments, USA) The V_G during the measurement was in the sub-threshold region. The I_{DS} was then converted to a ΔV_T based on the transfer curve.

2.3. E. coli metabolism kinetics measurement

In our experiments, we first measured a ΔV_T baseline for bacterial growth kinetics in a fresh culture medium (LB with 1 wt% of glucose) without antibiotic. During the baseline measurement, bacteria suspensions were added to the culture medium at $t = 0$ min and ΔV_T of the SiNWFETs were recorded in real-time.

2.4. Bacterial strains and growth conditions

Bacterial strains used in this study belong to *Escherichia coli* K12, *Staphyloccoccus saprophyticus* and *Staphylococcus aureus* and are listed in Table 1. Bacterial strains were grown in LB at 37 °C shaking 200 rpm (revolutions per minute). Antibiotics were used at the following concentrations if not stated otherwise AMP 100 mg/L, CEF 20 mg/L and CIP 1 mg/L.

2.5. E-test

Bacterial susceptibility to antibiotics was determined using E-test according to the instructions of the manufacturer (BioMérieux, France) on Mueller-Hinton agar (Sigma).

Table 1
Bacterial strains used in this study.

Strain number	Genotype
SK2	*Escherichia coli* K12 MG1655
SK3786	*Escherichia coli* K12 BW25113 *lacA::CTX-M-15*
SK4582	*Escherichia coli* MG1655 *lacIZYA::bla*
SK4686	*Escherichia coli* K12 MG1655 *gyrA2*-D87N (LM534)
SK4687	*Staphylococcus saprophyticus*
SK5276	*Staphylococcus aureus* C4–06

2.6. AST Protocol

All AST runs described in this paper were conducted according to following protocol. Bacteria were grown overnight in LB at 37 °C shaking 200 rpm. The chip was connected to measurement setup via probecard and the transfer characteristics as well as the I_{DS} vs. time with only culture medium (LB + 1 wt% glucose, 80 μL) at 37 °C was measured until a stable baseline was achieved. 100 uL of the bacterial sample was centrifuged at 1950g (rcf) for 3 min and re-suspended in 20 μL of fresh culture medium. Next 20 μL bacteria sample either with or without antibiotics was added to the 80 μL culture medium and the I_{DS} vs. time curve was measured.

2.7. Viable counts

Viable counts were performed in parallel with the electrical measurement. The bacterial suspension was diluted in PBS and appropriate dilutions were spread on LB agar. The number of colonies forming units (cfu) was calculated after overnight incubation in 37°C and the original amount of bacteria in each suspension was determined by multiplying the number of cfu with the dilution factor. Samples for determining τ via viable counts were treated identically as for measurement in the AST device except in a 96-well microtiterplate.

3. Results

3.1. Sensor design and electrical characteristics

SiNWFET sensors were fabricated on silicon-on-insulator (SOI) wafers using standard silicon process technology. Detailed process flow can be found in Section 2.1. The SiNWFET has heavily n-doped source/drain terminals (S/D) and lightly p-doped SiNW channel. The channel dimensions are 100 nm, 120 nm, and 1 μm in width, height, and length, respectively. A 5 nm-thick HfO_2 grown by atomic layer deposition (ALD) is employed as both the gate oxide and H^+-selective layer for the SiNWFET sensor. HfO_2 as a sensing layer has a near-Nernstian *p*H sensitivity and its *p*H sensitivity is weakly affected by the ionic strength in the solution [25]. During our experiments, pre-cultured bacterial samples were re-suspended in a culture medium (Luria-Bertani broth (LB) with 1 wt% of glucose) and then loaded into a polydimethylsiloxane (PDMS) container (~ 100 μL in volume) placed on top of the chip. As seen in Fig. 1c, S/D of the SiNWFET sensors are accessed through the metal pads along the chip edges using a probe card. Gate voltage (V_G) was applied via a Ag/AgCl reference electrode inserted in the culture medium. The chip holder is temperature controlled and can maintain a constant temperature of 37 °C inside the PDMS container. To avoid excessive evaporation, the culture medium was sealed by a layer of mineral oil during measurement.

Transfer characteristics for a SiNWFET measured in culture medium can be found in Fig. S1a. The SiNWFET has a n-type channel and exhibits a subthreshold swing (*SS*) of ~90 mV/dec with an on-to-off current ratio (I_{on}/I_{off}) of ~10^4 (Note S1a). ΔV_T vs. time (*t*) curve of a SiNWFET sensor measured in different *p*H buffer solutions is shown in Fig. 1d. V_T of the SiNWFET shifts positively with decreasing *p*H, showing a near-Nernstian response with a sensitivity of 59.0 ± 0.3 mV/pH (Fig. 1d inset), which is significantly higher than those using SiO_2 as the sensing layer [26], [27]. The *p*H response curve of the SiNWFET could later serve as calibration for analyzing the culture medium acidification induced by bacterial metabolism.

3.2. Rapid AST for E. coli

In this section, *E. coli* (Gram-negative) is used as the model pathogen for AST demonstration with SiNWFET sensors. SiNWFET V_T shift ΔV_T during bacteria culturing correlates linearly to the Δ*p*H of the culture medium which is a direct measure of the acidification induced by

bacterial metabolism [16], [28] (Note S1). During AST, the metabolic activity of susceptible bacteria will be greatly hindered by the antibiotic therefore the corresponding ΔV_T vs. t curve will differ significantly from that for the resistant bacteria. Susceptibility of *E. coli* to three antibiotics, i.e., ampicillin (AMP), cefotaxime (CEF), and ciprofloxacin (CIP), were first investigated using E-test as a reference, and the minimal inhibitory concentration (MIC) determined by E-test can be found in Table S1. The initial density of *E. coli* in the culture medium used for our SiNWFET based AST is $\sim 2.2 \times 10^9$ cfu/mL, as confirmed by cell plating performed in parallel. ΔV_T vs. t curves for the susceptible *E. coli* in response to 100 mg/L (33 × MIC) AMP, 20 mg/L (22 × MIC) CEF, and 1 mg/L (125 × MIC) CIP are shown in Figs. 2a, b, and 2c, respectively. The shaded areas along the solid lines depict the standard deviations calculated from 3 biological replicates with each replicate being averaged with data from 3 to 4 sensors. The small deviations between the biological replicates reflect good reliability and reproducibility of our SiNWFET sensors. Importantly, the susceptibility of *E. coli* to all the three antibiotics can be determined in less than 25 min, where the ΔV_T vs. t curve for antibiotic-treated sample (red lines) deviates significantly from the reference sample (black lines) without antibiotic treatment.

Same set of ASTs are also performed for AMP-resistant (AmpR, *E. coli bla*), CEF-resistant (CefR, *E. coli ctx-M-15*), and CIP-resistant (CipR, *E. coli gyrA*) *E. coli*. The results are respectively shown in Fig. 2d, e, and f. ΔV_T vs. t curves for the AmpR, CefR, and CipR *E. coli* show negligible difference between the antibiotic-treated and the reference samples. The results demonstrate that our SiNWFET sensors could clearly distinguish susceptible and resistant bacterial strains.

3.3. Differentiation of action mechanisms for antibiotics

In this section, we show that the action mechanisms of antibiotics can also be resolved by profiling the bacterial metabolism with the SiNWFET sensors. It is worth noting that such difference is very difficult to detect with conventional proliferation-based approaches as seen in Fig. 2a, b, and c (red lines).

ΔV_T response curves exhibit different patterns for susceptible *E. coli* under different antibiotic treatments (see red lines in Figs. 2a, 2b, and 2c). As known, AMP and CEF belong to the β-lactam antibiotic family that can lyse bacterial cells by inhibiting the synthesis of cell wall. One common feature for AMP and CEF treated *E. coli* samples is that ΔV_T decreases at the later stage of the measurement as seen in Fig. 2a and b. Such decrease in ΔV_T indicates *p*H increase and alkalization in the culture medium, which is likely due to release of cell cytoplasm as a result of the cell lysis by AMP and CEF. In particular, AMP exhibits a faster onset of bactericidal action and a higher killing rate in comparison to CEF as evidenced by its shorter response time and more significant reduction in the acidification rate (R_H) at the initial stage. This could be explained by that the two antibiotics differ in their binding affinity to different penicillin-binding proteins (PBPs) which play essential role in bacterial wall synthesis [29]. Consequently, they exhibit different bactericidal activity for *E. coli*.

On the other hand, CIP functions through inhibition of the DNA topoisomerase and gyrase and hinders bacteria's replication and reparation of DNA [30], [31]. The absence of the cell lysing process for CIP is reflected on the ΔV_T vs. t curve as no such alkalization and decrease of ΔV_T is observed. Interestingly, the ΔV_T curve for susceptible *E. coli* has a sharp drop immediately after addition of CIP with a higher concentration, i.e., 4 mg/L, as seen in Fig. S2a (red line). Such drop in ΔV_T is not shown on the response curve of the CipR *E. coli* (Fig. S2b) therefore is ascribed to the response of susceptible *E. coli* to CIP (not an artifact). A plausible explanation could be that high concentration of CIP induces stress on *E.coli* cells which quickly changes their metabolic pathway [32].

3.4. AST for Gram-positive bacteria

ASTs for Gram-positive bacterial strains, i.e., *S. aureus* and *S. saprophyticus*, were also studied to demonstrate the universality of our

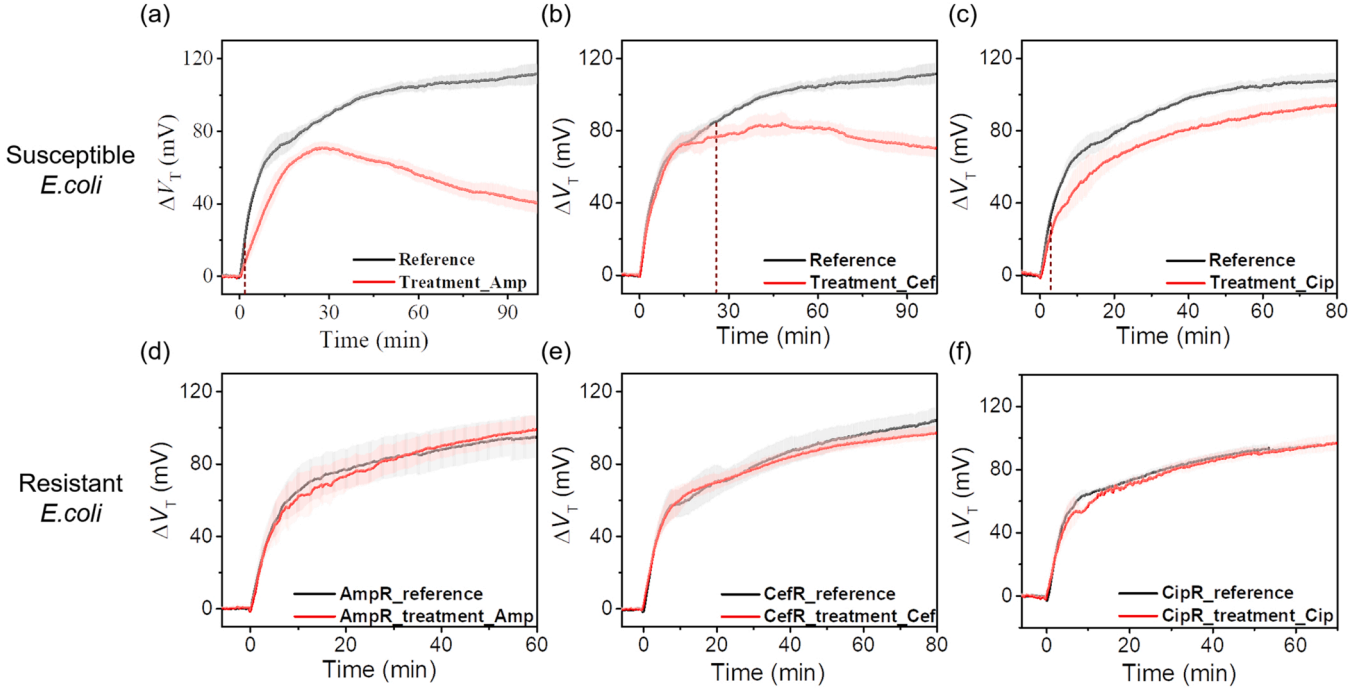

Fig. 2. ASTs for *E. coli* using SiNWFET sensors. ΔV_T vs. t curves for susceptible *E. coli* in response to: (a) AMP (100 mg/L), (b) CEF (20 mg/L), and (c) CIP (1 mg/L). (d), (e), and (f) plot the ΔV_T vs. t curves for resistant *E. coli* in response to AMP, CEF, and CIP, respectively. The black solid lines are *E. coli* culturing reference curves measured without antibiotics. The shaded areas along the solid lines depict the standard deviations calculated from 3 biological replicates with each replicate being averaged with data from 3 to 4 sensors. The dashed dark red lines in a, b, and c marked the response time for the antibiotic treatment.(For interpretation of the references to colour in this figure, the reader is referred to the web version of this article.)

AST approach. Fig. 3a depicts the reference ΔV_T vs. t curves for *E. coli*, *S. aureus*, and *S. saprophyticus* measured without antibiotics. The three bacteria have different acidification rate during culture as revealed by the difference in their ΔV_T slope, i.e., $d\Delta V_T/dt$, with an order of *E. coli* > *S. aureus* > *S. saprophyticus*. It is worth noting that, despite the difference in slope, ΔV_T for all three bacteria saturates at ~ 120 mV. This corresponds to decrease of 2 *p*H units approximately from 7 to 5, beyond which the culture medium likely becomes too acidic (*p*H < 5) to be changed by the cell metabolism.

S. saprophyticus and *S. aureus* responded rapidly to CIP (4 mg/L, 16 × MIC) which functions by hindering DNA replication and reparation, as shown by the immediate ΔV_T drop after the addition of CIP for both bacterial strains in Fig. 3b and c (blue lines). However, no significant differences were observed between the reference (black line) and the AMP-treated sample (red line) in Fig. 3b and c within the measurement duration, i.e., ~ 90 min for *S. aureus* and ~150 min for *S. saprophyticus*. In contrast to *E. coli*, *S. aureus* and *S. saprophyticus* are Gram-positive bacteria and are known to have thick cell-wall which could delay the cell response to AMP and take longer time to be lysed. To confirm this hypothesis, OD600 measurements were performed and showed that 70 and 125 min were needed for AMP to respectively affect the growth of *S. aureus* and *S. saprophyticus* (Fig. S3c and S3d). Meanwhile, cell lysis was not observed during the 3-hour monitoring time. Due to the slow biological process, the *p*H of the culturing medium reaches saturation before the cell response to AMP. Therefore, bacterial susceptibility to AMP is not detected within the measurement window. Clearly, such aspect needs to be carefully considered for AST design. One mitigation strategy would be to reduce the initial bacteria cell density so the time to reach *p*H saturation becomes longer. Despite this challenge, our sensors clearly detected that *S. aureus* and *S. saprophyticus* both respond faster to CIP than to AMP.

3.5. Determination of initial E. coli density N_0

Once the H^+ concentration is above the threshold, ΔV_T will increase until the culture medium reach *p*H 5. The onset time, t_{on}, is determined as the point where *p*H change reaches 0.1 unit (ΔV_T ~ 6 mV) (See Fig. S4a). A plot of N_0 vs. t_{on} is shown in Fig. S4b. As seen, t_{on} increases at lower N_0 since longer time is required to exceed the threshold. The curve of N_0 vs. t_{on} (Fig. S4b) can also work as the calibration curve for determining the N_0 of an unknown sample. As a demonstration, we first measured the ΔV_T vs. t curve for an *E. coli* sample with an unknown concentration (see dashed line in Fig. S4a) and the measured t_{on} is 2.6 h. This t_{on} corresponds to N_0 of 3.8×10^5 cfu/mL according to the calibration curve (as marked as the dashed line in Fig. S4b), which is close to the value of 5.6×10^5 cfu/mL measured by viable counts. In real diagnostics, especially for urinary tract infections (UTIs), it is important to determine the number of bacteria in the sample for doctors to discriminate between contamination and actual UTI.

3.6. Analysis of E. coli metabolic kinetics during growth

The H^+ ion concentration in the culture medium at time t, $H(t)$, can be calculated through

$$H(t) = H_0 \bullet 10^{\Delta V_T(t)/S}, \quad (1)$$

where H_0 is the initial H^+ ion concentration at $t = 0$ h, i.e., $H_0 = 6 \times 10^{16}$ H^+/L for *p*H = 7.0, $\Delta V_T(t)$ the SiNWFET sensor signal at time t, and S the *p*H sensitivity in mV/*p*H. The ISFET signal can be converted to $H(t)$ as shown in Fig. 4b.

Acidification rate $R_H(t)$ of the culture medium can be expressed as

$$R_H(t) = \frac{dH(t)}{dt} = \frac{H_0 \bullet 10^{\Delta V_T(t)/S}}{S} \bullet \frac{d\Delta V_T(t)}{dt} \quad (2)$$

On the other hand, $R_H(t)$ is the product of cell number $N(t)$ and H^+ production rate per cell v,

$$R_H(t) = N(t) \bullet v. \quad (3)$$

At the highest N_0, i.e., 2.0×10^9 cfu/mL, *E. coli* cells are in stationary phase and $N(t)$ remains essentially constant, which is also confirmed by viable cell counting (Fig. S5a). The $R_H(t)$ vs. t curve (Fig. S5b) is also quite stable after 10 min upon addition of *E. coli*. For the samples with lower N_0, the bacterial growth is in the log-growth phase. $N(t)$ can be described as

$$N(t) = N_0 \bullet 2^{t/\tau}. \quad (4)$$

Here τ is the cell doubling time of *E. coli*. Combining Eqs. 3 and 4, one can derive

$$\log_2^{R_H(t)} = \frac{1}{\tau} \bullet t + \log_2^{N_0 \bullet v}. \quad (5)$$

The τ can be obtained by viable cell counting and the doubling time of R_H, τ_H, can be extracted from the slope of the linear fitting of $\log_2^{R_H(t)}$ vs. t curve. Therefore, if v is constant, τ_H should be the same as the cell doubling time τ.

As seen from Fig. 4c, linear changes of $\log_2^{R_H(t)}$ vs. t curves are indeed observed. The τ_H extracted from the slopes of the $\log_2^{R_H(t)}$ vs. t curves are plotted in Fig. 4d. τ_H is relatively stable, i.e., 10–12 min, when N_0 is above 10^5 cfu/mL. It becomes longer for lower N_0, i.e., 16 and 23 min for N_0 at 6.0×10^4 and 2.9×10^3 cfu/mL. Interestingly, the extracted τ_H are generally shorter than the τ for *E. coli* measured by viable cell

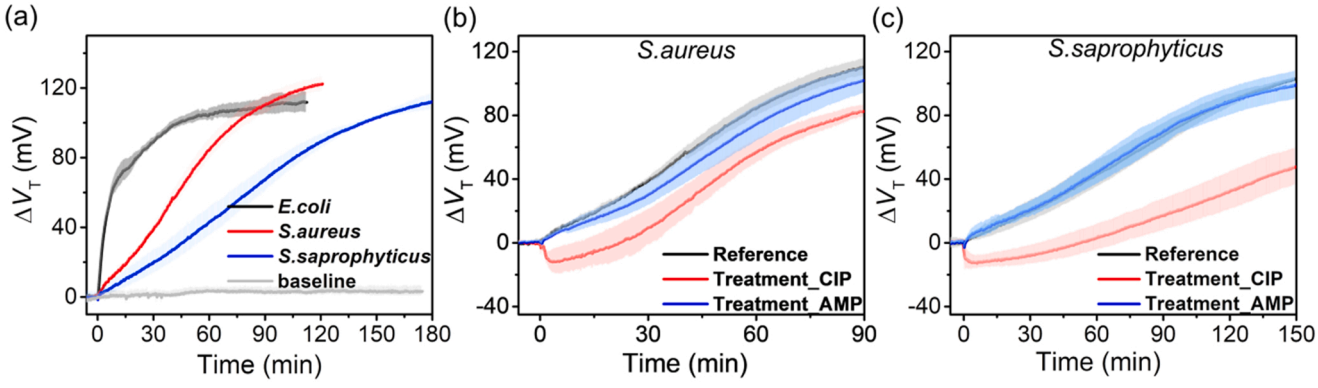

Fig. 3. (a) ΔV_T vs. t curves measured without antibiotics for *E. coli*, *S. aureus*, and *S. saprophyticus* with initial concentrations of 2.2×10^9, 2.5×10^9 and 3.6×10^9 cfu/mL, respectively. Sensor baseline measured with culture medium only (no bacteria cells) is also included. CIP (4 mg/L, red lines) and AMP (100 mg/L, blue lines) susceptibility tests for (b) *S. aureus* and (c) *S. saprophyticus*. The black lines in (b) and (c) are for reference runs measured without antibiotic. The shaded areas along the solid lines depict the standard deviations calculated from 3 biological replicates and each biological replicate containing result from 3 to 4 sensors.

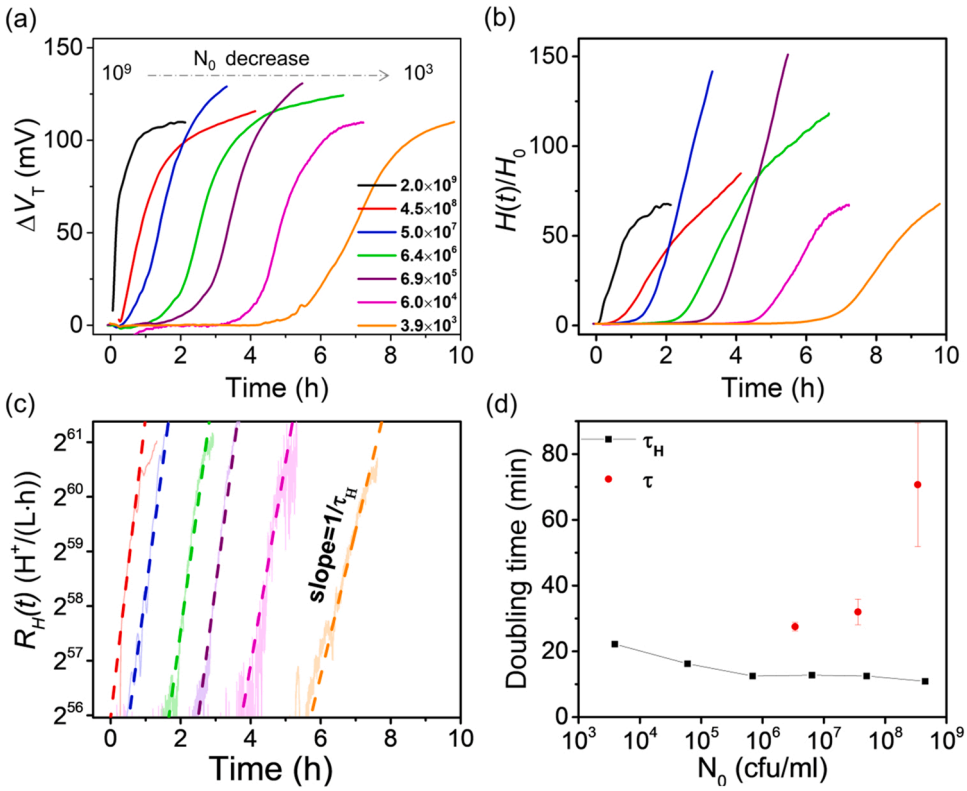

Fig. 4. (a) ΔV_T, (b) relative change in $H(t)$, i.e., $H(t)/H_0$, and for *E. coli* samples with different initial densities. Each curve was obtained by averaging the results from 3 to 4 devices using one biological sample. (c) $R_H(t)$ vs. t (y-axis in semi-log$_2$ scale). The shallow solid lines are the raw data and the dashed lines are the linear fitting curves. (d) τ_H (black) extracted from the slope of $R_H(t)$ vs. t curves and τ (red symbols) extracted from the growth curves by viable counts.

counting (Fig. S5). These results indicate that the H^+ production rate per cell, v, increases (instead of being constant) with t and cell density during culturing. To our best knowledge, this phenomenon has not been reported in the literature. One plausible explanation could be that cell growth and death could both take place when the cell density is high, and the dead cell could act metabolic adjuvants to stimulate cell metabolism. This leads to increasing v with t and cell density. Dedicated research is still needed to discover the real biological mechanism behind this phenomenon. These results show that our sensors can provide detailed information on the kinetics of bacterial metabolism.

4. Discussion

In contrast to growth-based phenotypic approaches, our AST relies on the acidification of culture medium induced by cell metabolism, which is rapid and universal, and particular advantageous for slow-growing bacterial strains. For slow growing strains it could take hours before a change in growth rate mediated by addition of an antibiotic is observable. The metabolism on the other hand, should be perturbed immediately just as in fast growing strains as long as the drug target is available in the cell. Our data support a fast metabolic response to at least two of the drugs tested, where the response to the antibiotics seems to occur within minutes. In this work, we use ΔV_T as the signal which is calibrated using the transfer characteristics of each individual sensor. Using ΔV_T fully excludes the influences due to variations of device characteristics and operation point. Consequently, the reliability and reproducibility of our ASTs are greatly improved in comparison to previous work in which current changes, ΔI_{DS}, were used as the readout signal [26], [28]. More detailed descriptions on ΔI_{DS}, ΔV_T as readout signals for a SiNWFET sensor can be found in Supplemental Information (Note S1). An example demonstrating sensor reproducibility is shown in Fig. S1c. Our results show that the SiNWFET sensors can rapidly determine the efficacy of AMP, CEF, and CIP for different bacterial strains. Apart from the rapid AST, the sensors could also differentiate the bactericidal mechanisms of the antibiotics and quantify the bacteria density in an unknown sample. The total assay could be accomplished within 30 min, including 5 min for sample centrifugation and resuspension and 25 min for the AST.

It is worth noting that the bacterial density used for our AST is high, i.e., ~2.2×10^9 cfu/mL, to achieve fast AST response. The AST time can be longer with lower cell densities (see Fig. S6). Practically, the high bacterial density can be realized by collecting bacterial cells into a microscale confined culture environment [10], [11]. Since the lateral dimension of our SiNWFET sensors is less than 1 μm, they can be easily integrated with microfluidics. The volume confinement in the microfluidics can generate high effective cell concentration with small bacterial amount for rapid ASTs. In addition, special design can be added to the microfluidic system to perform sample pre-filtering [11], sorting [18], which could potentially enable direct testing of the real sample without the need of any additional sample preparation step (such filtering and pre-cultivation).

Our SiNWFET sensors could also be functionalized to detect other specific elemental ions and small molecules that are produced in different metabolic processes. Such capability ensures the universality of our AST approach. Finally, we would like to emphasis that, regardless of what metabolic markers the sensors are targeting, the AST approach presented in this work is all-electrical, label-free and fully compatible with silicon CMOS technology, therefore is a promising solution for low-cost POC applications.

5. Conclusions

In a summary, we have demonstrated that SiNWFET sensors could deliver rapid AST results with a total assay time of less than 30 min for different bacterial strains, i.e., *E. coli*, *S. aureus*, and *S. saprophyticus*. Apart from the rapid AST, the sensors could also differentiate

bactericidal mechanisms for antibiotics with different modes of actions, and quantify the bacteria density in an unknown sample. We have also shown that acidification kinetic parameters can be quantitatively determined by the readout from the sensors. Our AST approach is label-free, all-electrical and fully compatible with silicon CMOS technology, therefore holds great promise for the development of a high throughput and low-cost POC device.

CRediT authorship contribution statement

Xingxing Xu: AST measurement, Research design, Data analysis, Writing – original draft. **Si Chen**: AST system set up, Data analysis, Writing – review and editing. **Yingtao Yu**: Silicon nano transistor fabrication. **Petra Virtanen**: Biologic experiment supporting. **Jiyue Wu**: Initial AST platform qualification. **Qitao Hu**: Silicon nano transistor fabrication. **Sanna Koskiniemi**: Biologic experiment supporting, Data analysis, Writing – review and editing, Research design, Funding acquisition. **Zhen Zhang**: Supervision, Research design, Data analysis, Writing – review and editing, Funding acquisition.

Declaration of Competing Interest

The authors declare that they have no known competing financial interests or personal relationships that could have appeared to influence the work reported in this paper.

Acknowledgments

This work is mainly supported by Olle Engkvist Foundation (196-0077). It is partially supported by the Swedish Strategic Research Foundation (FFL15-0174), Swedish Research Council (2019-04690) and the Wallenberg Academy Fellow program (2015-0127).

Appendix A. Supporting information

Supplementary data associated with this article can be found in the online version at doi:10.1016/j.snb.2022.131458.

References

[1] V.M. D'Costa, et al., Antibiotic resistance is ancient, Nature 477 (7365) (. 2011), 7365, https://doi.org/10.1038/nature10388.
[2] C.L. Ventola, The antibiotic resistance crisis, Pharm. Ther. 40 (4) (. 2015) 277–283. PMID: 25859123; PMCID: PMC4378521.
[3] H.C. Neu, The crisis in antibiotic resistance, Science 257 (5073) (. 1992) 1064–1073, https://doi.org/10.1126/science.257.5073.1064.
[4] Antibiotic-Resistant Infections Threaten Modern Medicine, Mod. Med., p. 2.
[5] C. Willyard, The drug-resistant bacteria that pose the greatest health threats, Nature 543 (7643) (. 2017), 7643, https://doi.org/10.1038/nature.2017.21550.
[6] Y.-Y. Liu, et al., Emergence of plasmid-mediated colistin resistance mechanism MCR-1 in animals and human beings in China: a microbiological and molecular biological study, Lancet Infect. Dis. 16 (2) (. 2016) 161–168, https://doi.org/10.1016/S1473-3099(15)00424-7.
[7] L.-L. Zhong, et al., Coproduction of MCR-1 and NDM-1 by colistin-resistant Escherichia coli Isolated from a healthy Individual, Antimicrob. Agents Chemother. vol. 61 (1) (. 2017), https://doi.org/10.1128/AAC.01962-16.
[8] S. Puttaswamy, S.K. Gupta, H. Regunath, L.P. Smith, S. Sengupta, A comprehensive review of the present and future antibiotic susceptibility, Test. AST Syst. Arch. Clin. Microbiol. 9 (3) (. 2018), https://doi.org/10.4172/1989-8436.100083.
[9] S.G. Jenkins, A.N. Schuetz, Current concepts in laboratory testing to guide antimicrobial therapy, Mayo Clin. Proc. 87 (3) (. 2012) 290–308, https://doi.org/10.1016/j.mayocp.2012.01.007.
[10] L.B. Reller, M. Weinstein, J.H. Jorgensen, M.J. Ferraro, Antimicrobial susceptibility testing: a review of general principles and contemporary practices, Clin. Infect. Dis. 49 (11) (. 2009) 1749–1755, https://doi.org/10.1086/647952.
[11] S.B. Debast, M.P. Bauer, E.J. Kuijper, European society of clinical microbiology and infectious diseases: update of the treatment guidance document for clostridium difficile infection, Clin. Microbiol. Infect. 20 (. 2014) 1–26, https://doi.org/10.1111/1469-0691.12418.
[12] H. Frickmann, W.O. Masanta, A.E. Zautner, Emerging rapid resistance testing methods for clinical microbiology laboratories and their potential impact on patient management, BioMed. Res. Int. 17 (2014), https://doi.org/10.1155/2014/375681 (Sep.).
[13] A. van Belkum, C.-A.D. Burnham, J.W.A. Rossen, F. Mallard, O. Rochas, W. M. Dunne, Innovative and rapid antimicrobial susceptibility testing systems, Nat. Rev. Microbiol. 18 (5) (2020), https://doi.org/10.1038/s41579-020-0327-x.
[14] G. Longo, et al., Rapid detection of bacterial resistance to antibiotics using AFM cantilevers as nanomechanical sensors, Nat. Nanotechnol. v8 (7) (. 2013) 522–526, https://doi.org/10.1038/nnano.2013.120. Art. no. 7.
[15] D.C. Spencer, T.F. Paton, K.T. Mulroney, T.J.J. Inglis, J.M. Sutton, H. Morgan, A fast impedance-based antimicrobial susceptibility test, Nat. Commun. 11 (1) (. 2020), https://doi.org/10.1038/s41467-020-18902-x.
[16] Y. Tang, L. Zhen, J. Liu, J. Wu, Rapid antibiotic susceptibility testing in a microfluidic pH sensor, Anal. Chem. 85 (5) (. 2013) 2787–2794, https://doi.org/10.1021/ac303282j.
[17] Ö. Baltekin, A. Boucharin, E. Tano, D.I. Andersson, J. Elf, Antibiotic susceptibility testing in less than 30min using direct single-cell imaging, Proc. Natl. Acad. Sci. 114 (34) (. 2017) 9170–9175, https://doi.org/10.1073/pnas.1708558114.
[18] H. Li, et al., Adaptable microfluidic system for single-cell pathogen classification and antimicrobial susceptibility testing, Proc. Natl. Acad. Sci. 116 (21) (2019) 10270–10279, https://doi.org/10.1073/pnas.1819569116.
[19] M. Wipf, et al., Selective sodium sensing with gold-coated silicon nanowire field-effect transistors in a differential setup, ACS Nano 7 (7,) (. 2013) 5978–5983, https://doi.org/10.1021/nn401678u.
[20] P. Bergveld, Thirty years of ISFETOLOGY: what happened in the past 30 years and what may happen in the next 30 years, Sens. Actuators B Chem. 88 (1) (. 2003) 1–20, https://doi.org/10.1016/S09254005(02)00301-5.
[21] Y. Yang, K. Gupta, K.L. Ekinci, All-electrical monitoring of bacterial antibiotic susceptibility in a microfluidic device, Proc. Natl. Acad. Sci. 117 (20) (2020) 10639–10644, https://doi.org/10.1073/pnas.1922172117.
[22] D. Zhang, et al., Direct assessment of solid–liquid interface noise in ion sensing using a differential method, Appl. Phys. Lett. 108 (15) (. 2016), 151603, https://doi.org/10.1063/1.4946857.
[23] J. Peter Jurtshuk, Bacterial Metabolism. University of Texas Medical Branch at Galveston, 1996. Accessed: Feb. 02, 2021. [Online]. Available: https://www.ncbi.nlm.nih.gov/books/NBK7919/.
[24] T. Dewettinck, K. Van Hege, W. Verstraete, Development of a rapid pH-based biosensor to monitor and control the hygienic quality of reclaimed domestic wastewater, Appl. Microbiol. Biotechnol. 56 (5–6) (. 2001) 809–815, https://doi.org/10.1007/s002530100705.
[25] S. Zafar, et al., Silicon nanowire field effect transistor sensors with minimal sensor-to-sensor variations and enhanced sensing characteristics, ACS Nano 12 (7) (. 2018) 6577–6587, https://doi.org/10.1021/acsnano.8b01339.
[26] B. Ibarlucea, T. Rim, C.K. Baek, J.A.G.M. de Visser, L. Baraban, G. Cuniberti, Nanowire sensors monitor bacterial growth kinetics and response to antibiotics, Lab Chip 17 (24) (2017) 4283–4293, https://doi.org/10.1039/C7LC00807D.
[27] X.P.A. Gao, G. Zheng, C.M. Lieber, Subthreshold regime has the optimal sensitivity for nanowire FET biosensors, Nano Lett. 10 (2) (. 2010) 547–552, https://doi.org/10.1021/nl9034219.
[28] M. Castellarnau, et al., ISFET-based biosensor to monitor sugar metabolism in bacteria, Mater. Sci. Eng. C 28 (5) (. 2008) 680–685, https://doi.org/10.1016/j.msec.2007.10.074.
[29] N.A. Curtis, D. Orr, G.W. Ross, M.G. Boulton, Affinities of penicillins and cephalosporins for the penicillin-binding proteins of Escherichia coli K-12 and their antibacterial activity, Antimicrob. Agents Chemother. 16 (5) (. 1979) 533–539, https://doi.org/10.1128/AAC.16.5.533.
[30] D.M. Campoli-Richards, J.P. Monk, A. Price, P. Benfield, P.A. Todd, A. Ward, Ciprofloxacin, Drugs 35 (4) (. 1988) 373–447, https://doi.org/10.2165/00003495-198835040-00003.
[31] D.C. Hooper, J.S. Wolfson, E.Y. Ng, M.N. Swartz, Mechanisms of action of and resistance to ciprofloxacin, Am. J. Med. 82 (4A) (1987) 12–20.
[32] P. Belenky, et al., Bactericidal antibiotics induce toxic metabolic perturbations that lead to cellular damage, Cell Rep. 13 (5) (. 2015) 968–980, https://doi.org/10.1016/j.celrep.2015.09.059.

XingXing Xu received B.S. degree from University of Science and Technology of China in 2015, and Ph.D degree from Uppsala University in 2020. She is currently a postdoc researcher at solid-state electronics at Uppsala University. Her research interests focus on electrochemical DNA sensor andantibiotic susceptible testing sensor using microfabricated devices.

Si Chen received the B.S. degree (2004) from University of Science and Technology of China and the M.S. degree (2007) from Shanghai Institute of Ceramics, Chinese Academy of Sciences, and Ph.D. degree (2013) in solid state electronics from Uppsala University, Sweden. He worked as a characterization and development engineer at Solibro Research AB from 2013 to 2016, and joined Uppsala University in 2016 as a researcher. His main research interest is novel device structures and materials for electronic biosensor applications.

Yingtao Yu received the B.S. degree (2018) from University of Science and Technology of China, and is currently a Ph.D. student at solid-state electronics at Uppsala University in Uppsala, Sweden. His research interests include nano-device for sensing application, piezoresistive NEMS and biosensors.

Petra Virtanen received her M.Sc. degree in Biology (2016) from Uppsala University, Sweden. She is currently pursuing her PhD in microbiology at the department of Cell and

Molecular Biology at Uppsala University. Her research focuses on finding new treatment options for bacterial infections through targeted eradication of bacterial pathogens.

Jiyue Wu is currently a postdoctral researcher at Fudan University, China. He received his B. Eng. Degree in Polymer Materials Science and Engineering from Donghua University (DHU) in 2015. He completed his Ph.D. degree in Materials Science at Queen Mary University of London (QMUL) in 2019. After that, he worked as a postdoctral reseracher at Uppsala University, Sweden. His research interest covers the development of advanced piezoelectric ceramics for energy storage and the investigation of piezoelectric nanomaterials for medical applications, including tumor treatment and neural regulation.

Qitao Hu received the B.S. degree (2015) from the University of Science and Technology of China and the Ph.D. degree (2021) at solid-state electronics at Uppsala University in Uppsala, Sweden. Currently, he works as a postdoctoral researcher at Uppsala University. His research topic is silicon-based nanodevices and their applications in biosensing, single-molecule analysis, and quantum sensing.

Sanna Koskiniemi is an associate professor at the department of Cell and Molecular Biology, Uppsala University, Sweden. Dr. Koskiniemi got her PhD from the medical faculty at Uppsala University in 2010. After her PhD she received several fellowships that allowed her to spend three years as a postdoctoral fellow at University of California Santa Barbara. In 2014 she got a tenure-track position at the faculty of science and technology at Uppsala university and received several starting grants including ERC that allowed her to start her own group. Her work focuses on understanding how and if bacterial toxin delivery plays a role in regulation of bacterial growth, communication, kin recognition, virulence and colonization of a host.

Zhen Zhang is a professor of solid-state electronics at Uppsala University in Uppsala, Sweden. He received the Ph.D degree in department of microelectronics and information technology from Royal Institute of Technology (KTH) of Sweden in 2008. He worked as a research staff member at IBM T. J. Watson research center at Yorktown Heights, New York from 2008 to 2013, and joined Uppsala University in 2013. His research interest covers semiconductor based electronic sensors, nanoscale semiconductor devices and bio-electronics.